Electronic Supporting Information

Synthesis of Silica Nanoparticles with Controllable Surface Roughness for Therapeutic Protein Delivery

Yuting Niu,[a] Meihua Yu,[a] Jun Zhang,[a] Yannan Yang,[a] Chun Xu,[a] Michael Yeh,[a] Elena Taran,[b] Jeff Jia Cheng Hou,[a] Peter P Gray[a] and Chengzhong Yu[,a]*

[a] Australian Institute for Bioengineering and Nanotechnology, The University of Queensland, Brisbane, QLD 4072, Australia.

E-mail: c.yu@uq.edu.au; Fax: +61-7-334 63973; Tel: +61-7-334 63283

[b] Australian National Fabrication Facility-QLD Node, Australian Institute for Bioengineering and Nanotechnology, The University of Queensland, Brisbane, QLD 4072, Australia.

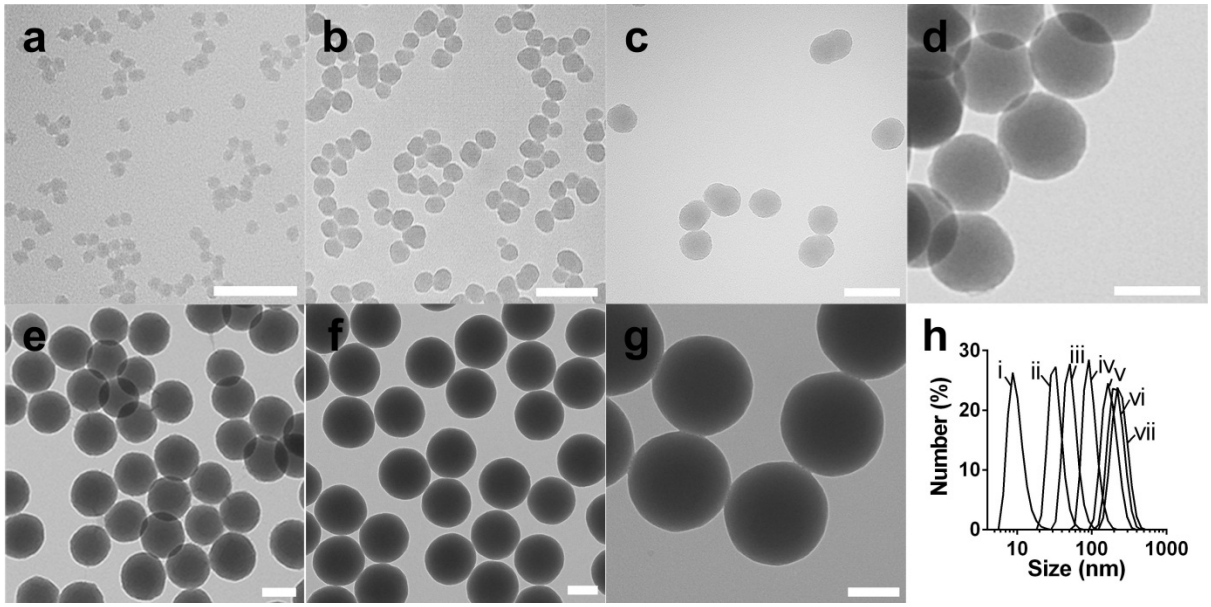

Figure S1. TEM images (a-g) and particle size distribution curves (f) of shell and core particles. Shell particles: a&h-i) 13nm, b&h-ii) 28nm, c&h-ii) 54nm, d&h-iv) 98nm, e&h-v) 135nm and f&h-vi) 175nm. Core particle: g&h-vii) 211nm. Scale bar: 100 nm

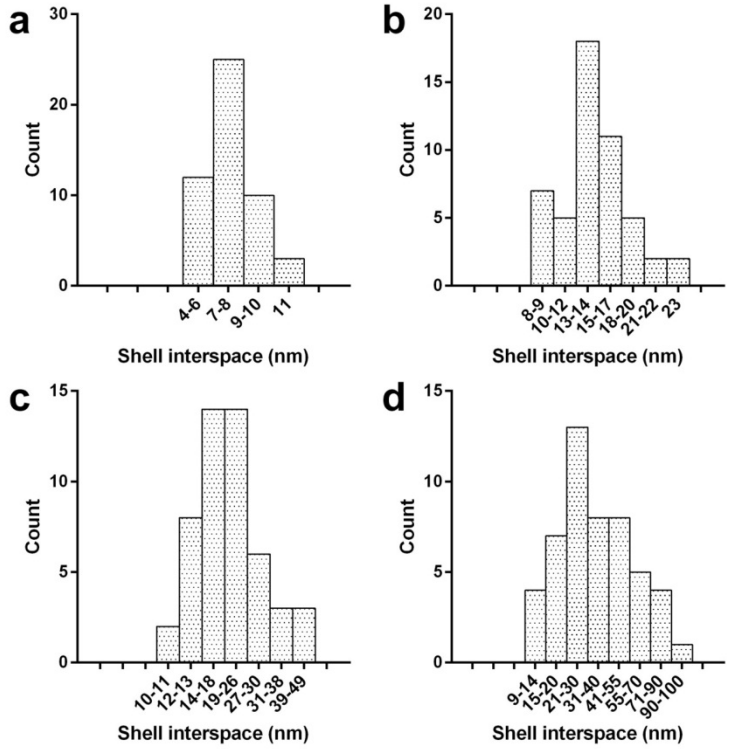

Figure S2. The interspace size of RSNs. a) RSN-211@13, b) RSN-211@28, c) RSN-211@54, d) RSN-211@98. The interspaces are measured from SEM images by recording 50 edge-to-edge interspacing data in each sample.

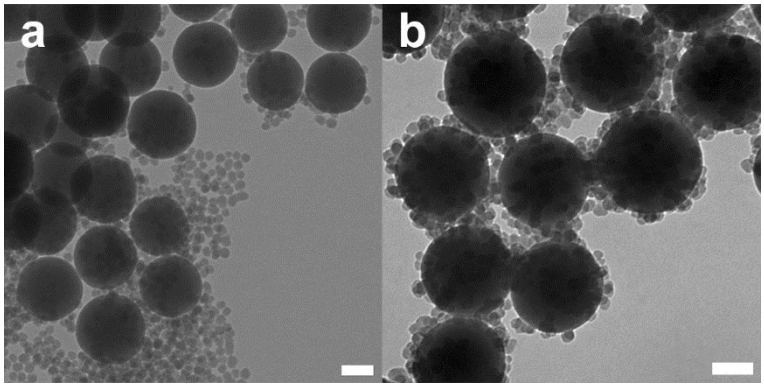

Figure S3. TEM images showing the synthesis of RSN-211@28 using previous recipe after washing and drying process (a) and in reaction solution (b). Scale bar: 100 nm

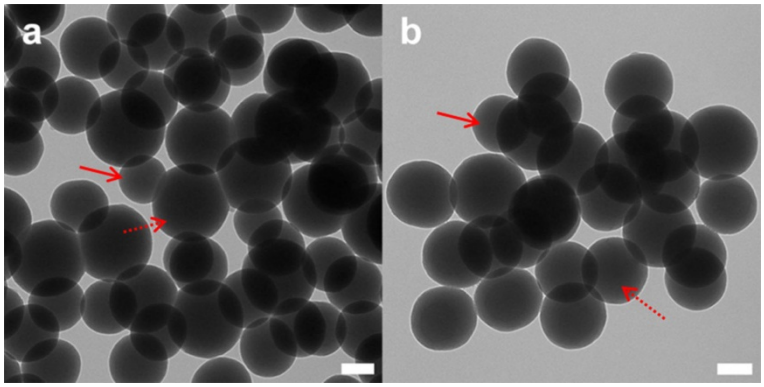

Figure S4. TEM images of failed synthesis of RSNs with much larger shell sizes. a) Core particles (dotted arrow) mixed with the shell of 135 nm (solid arrow), b) Core particle (dotted arrow) mixed with the shell of 175 nm (dotted arrow). Scale bar: 100 nm.

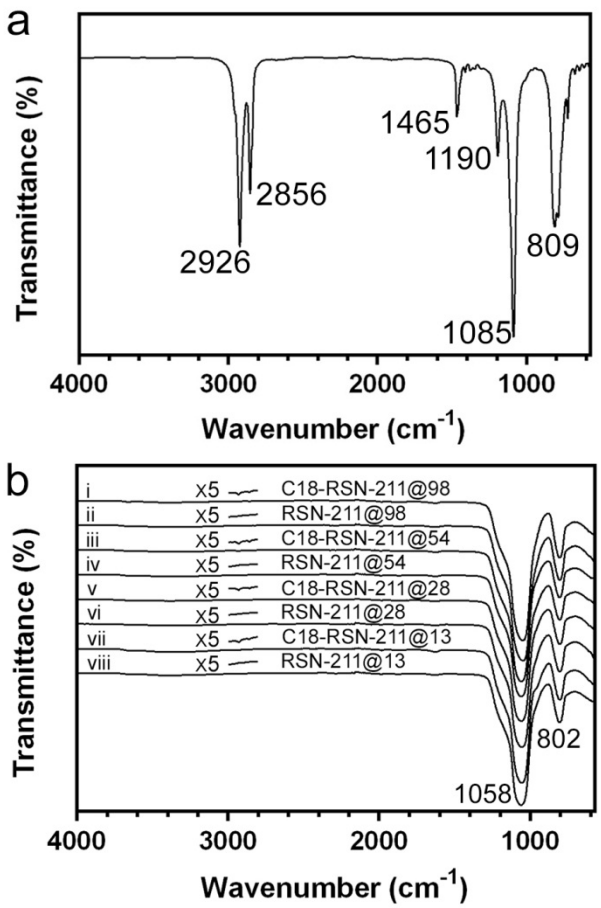

Figure S5. Fourier transform infrared (FTIR) spectra of pure liquid n-ODMS (a) and a series of RSNs with and without hydrophobic modification (b).

The RSNs before and after modification of octadecyl group is characterized by FTIR technique. Figure S5a shows the FTIR spectrum of pure liquid n-ODMS, where the six characteristic peaks at 809, 1085, 1190, 1465, 2856 and 2926 cm^{-1} can be attributed to ν(Si-O), ν(C-O)+ ν(C-C), ρ(CH_3), δ(C-H)[1] and symmetric and anti-symmetric -CH_2- stretching,[2, 3] respectively. All the spectra of silica nanoparticles show the same characteristic bands at 802 cm^{-1} and broad band centrated at 1058 cm^{-1}, suggesting –Si-O-Si- bonding.[4] In the spectra of all silica nanoparticles after hydrophobic modifications (Figure S5b i, iii, v, vii), two extra peaks at 2856 and 2926 cm^{-1} can be observed, shown as the curves enlarged by 5-folds, which can be attributed to symmetric and anti-symmetric -CH_2- stretching, respectively, indicating the successful modification of octadecyl groups.[5]

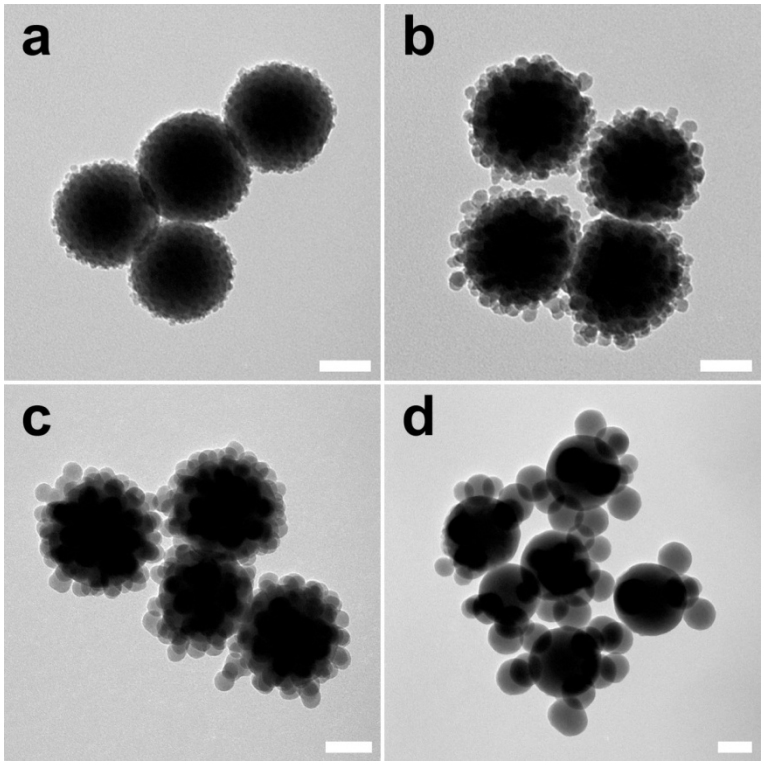

Figure S6. TEM images of hydrophobic modified RSNs. a) C18-RSN-211@13, b) C18-RSN-211@28, c) C18-RSN-211@54 and d) C18-RSN-211@98 (d). Scale bar: 100 nm.

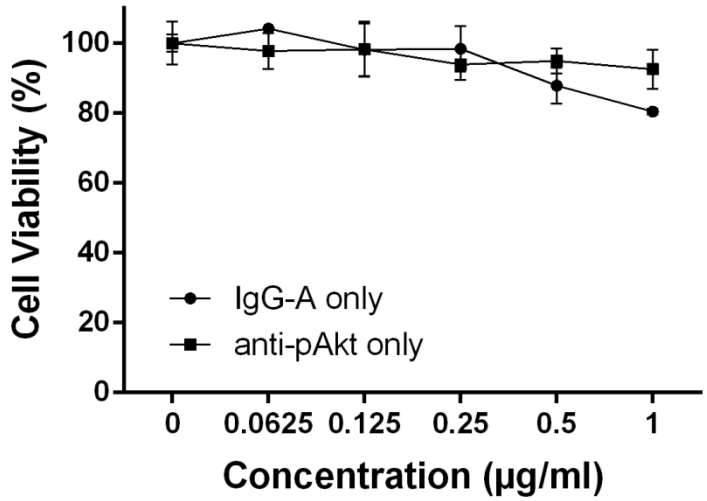

Figure S7. Cell viability of MCF-7 cells incubated with varying concentrations of non-specific IgG-A (●) only and anti-pAkt antibody (■) only, respectively. Data represent mean ± SD.

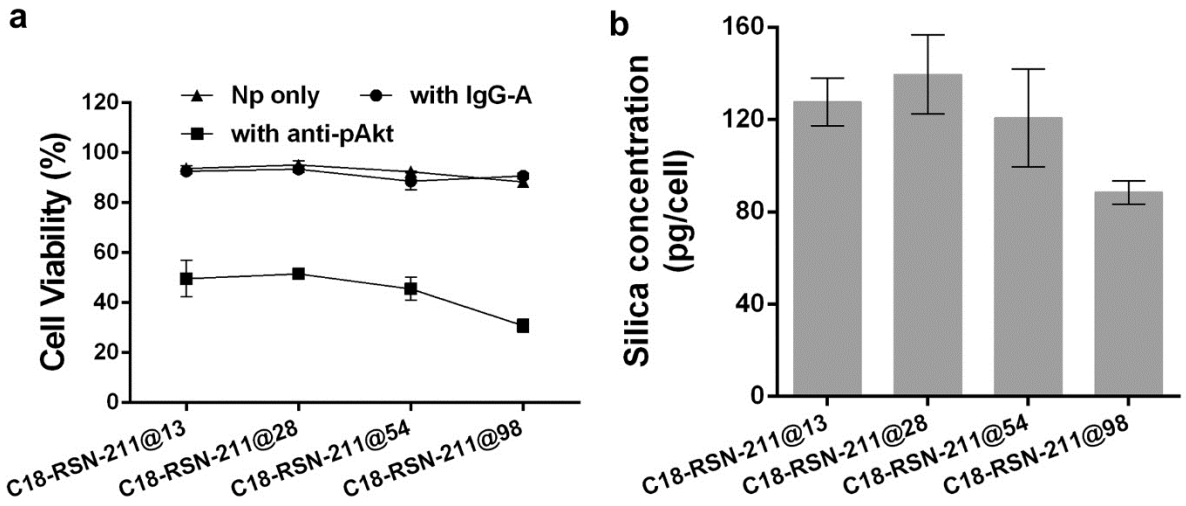

Figure S8. The comparison of anti-pAkt antibody delivery efficiency (a) and cellular uptake performance of C18-RSNs measured by ICPOES (b). Data represent mean ± SD.

C18-RSN-211@13, C18-RSN-211@28 and C18-RSN-211@54 were also used apart from C18-RSN-211@98 to deliver anti-pAkt antibody into cells. Both C18-RSNs alone or loaded with non-specific IgG-A did not cause significant cell inhibition. Equal amount of C18-RSNs (50 μg) was mixed with excessive amount of anti-pAkt antibody (1 μg) in PBS solution to ensure a saturated adsorption. At the nanoparticle concentration of 15 μg ml-1, cell viability decreases to 50%, 51% and 46% using C18-RSN-211@13, C18-RSN-211@28 and C18-RSN-211@54 as nano-carriers, respectively, while C18-RSN-211@98+anti-pAkt induces a lower cell survival rate to 31% (Figure S8a). This difference is attributed to the combined effects of two factors: the cellular uptake efficiency and protein adsorption ability. As shown in Figure S8b, averagely 127, 139, 121 and 88 pg of silica from C18-RSN-211@13, C18-RSN-211@28, C18-RSN-211@54 and C18-RSN-211@98 is taken up by each cell, respectively, because nanoparticles with larger sizes have lower cell penetration.[6-8] This trend is opposite to the adsorption trend (Fig. 3), where C18-RSN-211@98 shows the highest adsorption ability to large protein (IgG-A). Consequently, the opposite trends of adsorption and cellular uptake lead to the highest cell inhibition of C18-RSN-211@98+anti-pAkt.

Table S1. Size and ζ potential characterizations of shell and core particles.

Sample	size (nm)		PDI[c]	ζ-potential (mV)
	TEM[a]	DLS[b]		
Shells	13±2	10±0.3	0.11±0.01	-42±2.4
	28±3	33±0.4	0.03±0.02	-42±8.3
	54±5	54±0.7	0.01±0.01	-53±2.6
	98±7	96±1.3	0.03±0.01	-53±1.0
	135±8	179±3.6	0.02±0.02	-33±1.9
	175±8	219±2.4	0.03±0.03	-32±0.9
Core	211±11	241±1.4	0.01±0.01	+31±0.2

[a]Mean size±SD of shell/core particles by recording 50 data from TEM images. [b]Number mean size ±SD of shell/core particles by DLS method. [c]Polydispersity index.

Table S2. Characterizations of RSNs with varied surface topography.

Sample ID	Size(nm)		PDI[c]	S_{BET} (m^2 g^{-1}) [d]	Interspace [e] (nm)
	TEM[a]	DLS[b]			
RSN-211@13	254±26	287±5	0.16±0.07	25.4	7±2
RSN-211@28	270±15	371±13	0.23±0.05	26.9	14±4
RSN-211@54	297±20	398±16	0.13±0	25.2	21±9
RSN-211@98	380±39	480±13	0.22±0.04	22.4	38±22

[a] Mean size±SD of RSNs by recording 50 data from TEM images. [b]Number mean size ±SD of RSNs by DLS method. [c]Polydispersity index of RSNs. [d] BET specific surface area of RSNs. [e] Mean interspace size ±SD of RSNs by recording 50 data from SEM images.

Table S3. Estimation of protein coverage on RSNs/C18-RSNs

Protein	Sample ID	N_{max}[a]	N_{ads}[b]	Coverage %[c]
Cytochrome *c*	RSN-211@13	3.59×10^{18}	2.55×10^{17}	7.11
	RSN-211@28	3.81×10^{18}	3.65×10^{17}	9.59
	RSN-211@54	3.56×10^{18}	3.38×10^{17}	9.49
	RSN-211@98	3.18×10^{18}	1.77×10^{17}	5.58
IgG-F	RSN-211@13	3.23×10^{17}	2.94×10^{17}	91.07
	RSN-211@28	3.43×10^{17}	3.22×10^{17}	94.02
	RSN-211@54	3.20×10^{17}	3.92×10^{17}	122.23
	RSN-211@98	2.86×10^{17}	3.41×10^{17}	117.65
IgG-A	RSN-211@13	8.08×10^{16}	5.08×10^{16}	62.90
	RSN-211@28	8.56×10^{16}	6.88×10^{16}	80.40
	RSN-211@54	8.02×10^{16}	7.26×10^{16}	90.59
	RSN-211@98	7.15×10^{16}	9.07×10^{16}	126.87
	C18-RSN-211@13	8.08×10^{16}	1.44×10^{17}	178.57
	C18-RSN-211@28	8.56×10^{16}	1.97×10^{17}	229.49
	C18-RSN-211@54	8.02×10^{16}	2.22×10^{17}	276.83
	C18-RSN-211@98	7.15×10^{16}	2.41×10^{17}	336.88

[a]N_{max} represents the theoretical number of protein molecules that is assumed to fully cover the surface of 1 gram of RSNs in a single-layered fashion.

$$N_{max} = \frac{S_{BET}(m^2\ g^{-1})}{\pi r_{protein}^{2}(m^2)} \quad (1)$$

[b]N_{ads} represents the actual number of protein molecules (calculated from adsorption amount, W_{ads}) that associated on the surface of 1 gram of RSNs/C18-RSNs. N_A stands for Avogadro constant, and $MW_{protein}$ shows protein molecular weight.

$$N_{ads} = \frac{W_{ads}(mg\ g^{-1}) \cdot N_A}{MW_{protein}} \quad (2)$$

[c]Coverage% represents the actual protein coverage percentages, compared to theoretical number of protein molecules where the surface is assumed to be fully covered in a single-layered manner.

$$coverage\% = {}^{N_{ads}}/_{N_{max}} \times 100\% \quad (3)$$

Table S4. SPR signal intensity.

Sample ID	without IgG-F(RU)	with IgG-F(RU)
RSN-211@13	-1.9	462.3
RSN-211@28	-3.8	531.2
RSN-211@54	-4	564
RSN-211@98	-2.6	527.5
PBS	-0.4	--

Note: SRP signal intensity was determined at the peak point 128 seconds after sample injection

Notes and references

1 M. I. Tejedor-Tejedor, L. Paredes and M. A. Anderson, *Chem. Mater*, 1998, **10**, 3410-3421.
2 Q. Wu, L. Wang and L. Zu, *J. Autom. Methods Manage. Chem.*, 2011, **2011**, 7.
3 K. Kailasam and K. Muller, *J. Chromatogr. A*, 2008, **1191**, 125-135.
4 D. B. Mahadik, A. V. Rao, A. P. Rao, P. B. Wagh, S. V. Ingale and S. C. Gupta, *J. Colloid Interf Sci*, 2011, **356**, 298-302.
5 J. Zhang, S. Karmakar, M. H. Yu, N. Mitter, J. Zou and C. Z. Yu, *Small*, 2014, **10**, 5068-5076.
6 F. Lu, S. H. Wu, Y. Hung and C. Y. Mou, *Small*, 2009, **5**, 1408-1413.
7 J. Zhu, L. Liao, L. N. Zhu, P. Zhang, K. Guo, J. L. Kong, C. Ji and B. H. Liu, *Talanta*, 2013, **107**, 408-415.
8 J. Rejman, V. Oberle, I. S. Zuhorn and D. Hoekstra, *Biochem J*, 2004, **377**, 159-169.